Noname manuscript No.
(will be inserted by the editor)

Robust Pseudo Virtual Passive Dynamic Walking with Control of Swing-leg Retraction

Fumihiko Asano

Received: date / Accepted: date

Abstract This paper proposes a simplified method of underactuated virtual passive dynamic walking without having any singularities in the control input, which is termed as the pseudo virtual passive dynamic walking (PVPDW), and analyzes the gait properties considering quasi-constraint on the impact posture. First, we introduce a planar underactuated biped model that added an upper body by means of a bisecting hip mechanism and formulate the method of PVPDW based on the concept of pseudo center of mass. Second, we introduce a control law for inhibiting swing-leg retraction and analyze the effect on the gait stability. The simulation results show that falling down as a 1-DOF rigid body dramatically increases the stable domain even though the hip angle at impact is not precisely kept constant. Finally, we discuss the mechanism from the energy-loss coefficient point of view.

Keywords Limit cycle walking · Swing-leg retraction · Bisecting hip mechanism

1 Introduction

Achieving robust dynamic walking is one of the basic subjects in the field of robotic bipedal locomotion, especially development of limit-cycle walkers. The definitions of the gait stability or robustness differ in accordance with the desired tasks. In limit-cycle walkers, however, the generated gait is said to be robust in the sense that the motion rapidly converges to the steady limit cycle or the stable domain of the initial condition is wide. In general, many bipedal

F. Asano
School of Information Science, Japan Advanced Institute of Science and Technology
1-1 Asahidai, Nomi, Ishikawa 923-1292, Japan
Tel.: +81-761-51-1243
Fax: +81-761-51-1149
E-mail: fasano@jaist.ac.jp

humanoids are controlled based on the specified control strategies, mainly zero moment point (ZMP) based approaches, and their robust motions are successfully accomplished. In contrast, limit cycle walkers are good examples for achieving energy-efficient walking but their gait stability is fragile. They usually generate dynamic gaits without using any desired trajectories, and the stable domain is not so wide. It is common understanding that there is a trade-off between the gait robustness and energy-efficiency, and it is not easy to achieve both properties simultaneously.

Virtual passive dynamic walking (VPDW) is one of the approaches to efficient bipedal locomotion [1]. By reproducing the driving mechanism of gravity effect in passive dynamic walking, simple walkers with small actuators can generate efficient gaits on level ground. In this method, however, the walkers must be fully-actuated and the problem of ZMP constraint then arises with ankle-joint actuation. Utilizing effects of semicircular feet is one of the solutions for avoiding the ZMP constraint; the rolling effect during the stance phases functions as a virtual ankle actuation and overcoming the potential barrier at mid-stance then becomes possible [2]. Semicircular feet also have the effect of shock-absorbing at impact and this helps reduction of energy consumption. In this case, VPDW is achieved only by hip-joint actuation and another problem arises with it. VPDW is specified as a redundant equation of the control torques and can be achieved by solving it in realtime. In underactuated VPDW, a singularity appears in the control input; this is the condition that the relative angular velocity of the hip becomes zero. Although the system automatically avoids the condition, the control torque significantly increases when approaching it. This paper then proposes a novel VPDW-like approach to efficient level gait generation of an underactuated biped without having any singularities in the control torque. Although the control input according to the pseudo VPDW is differently given and is simpler than the original VPDW, the restored mechanical energy discretely behaves in the same manner as VPDW. We numerically investigate the validity and propose a robust control law utilizing the reference trajectory of mechanical energy.

On the other hand, it has been suggested that the impact conditions play important roles in generation of stable limit cycles. There are several results focusing on the effect of swing-leg retraction (SLR); this is a phenomenon that the swing leg moves backward just prior to impact in walking or running [3]. In [4][5], it is described that the effect of SLR helps limit cycle stability and some mathematical evidences are produced. In contrast, Ikemata et al. experimentally confirmed that constraining the impact posture is effective for enhancing the limit cycle stability [6]. By applying a mechanical stopper to a kneed passive-dynamic walker, they successfully achieved long-time walking on a treadmill. Although the results are controversial, the effect of impact must be an important factor in stabilization of limit cycles. Another subject in this paper is to discuss the effect of SLR on the stability of limit cycle walking. We propose a simple control law of SLR and numerically investigate the effect on the stability and gait properties based on some criteria.

This paper is organized as follows. Firstly, the model of an underactuated biped with an upper body incorporating a bisecting hip mechanism is described in Section 2. In Section 3, the method of pseudo VPDW is introduced and its simplification is considered. In Section 4, a simple control of SLR is proposed and the validity is numerically verified. In Section 5, the gait properties are numerically analyzed and the advantageous of the control of SLR is investigated from the energy-loss coefficient point of view. Section 6 concludes this paper and describes future research directions.

2 Modeling of Underactuated Biped with Upper Body

This section describes the bisecting hip mechanism (BHM) and discusses its feasibility through development of a prototype.

2.1 Bisecting Hip Mechanism

Fig. 1 shows an overview of our prototype BHM. Although there are many approaches to realize a BHM, we did so with sprockets and chains. A sprocket is attached to the inner leg, and its rotational motion is inversely transmitted to another sprocket in the body through chains wound in the shape of the letter "S". One S chain loosens when the other stretches, so there exists a dead-band and backlash around the standing posture. This is a crucial problem from a practical point of view but would be considerably resolved by installing tension pulleys or by using timing belts instead of metallic chains. The rotational motion of the sprocket is then transmitted forward to another one attached to the outer leg through another chain. The outer and inner legs then symmetrically move in opposite to each other with respect to the torso. Fig. 2 shows the symmetric motion of the legs. We can smoothly move two legs and maintain the posture at any angle. Back-drivability is almost completely achieved.

In passive stabilization of the upper body, the use of springs is also an effective way [7]. For reduction of the DOF, however, the rigid mechanical constraint provided by a BHM is more suitable.

2.2 Dynamic Equation

We deal with a planar underactuated biped model with semicircular feet and a torso as shown in Fig. 3. We add a 1-link torso as the upper body to the biped incorporating a BHM. Its mass and inertia moment are m_T [kg] and I_T [kg·m^2]. The joint torques between the torso and stance-leg, u_1, and swing-leg, u_2, are known. The central point of the foot circle is positioned on the leg link, and the foot radius is R [m]. Let $\boldsymbol{\theta} = \left[\, \theta_1 \ \theta_2 \ \theta_3 \,\right]^{\mathrm{T}}$ be the generalized coordinate vector; the dynamic equation of the biped model then becomes

$$\boldsymbol{M}(\boldsymbol{\theta})\ddot{\boldsymbol{\theta}} + \boldsymbol{h}(\boldsymbol{\theta}, \dot{\boldsymbol{\theta}}) = \boldsymbol{S}\boldsymbol{u} + \boldsymbol{J}_H^{\mathrm{T}}\lambda_H, \tag{1}$$

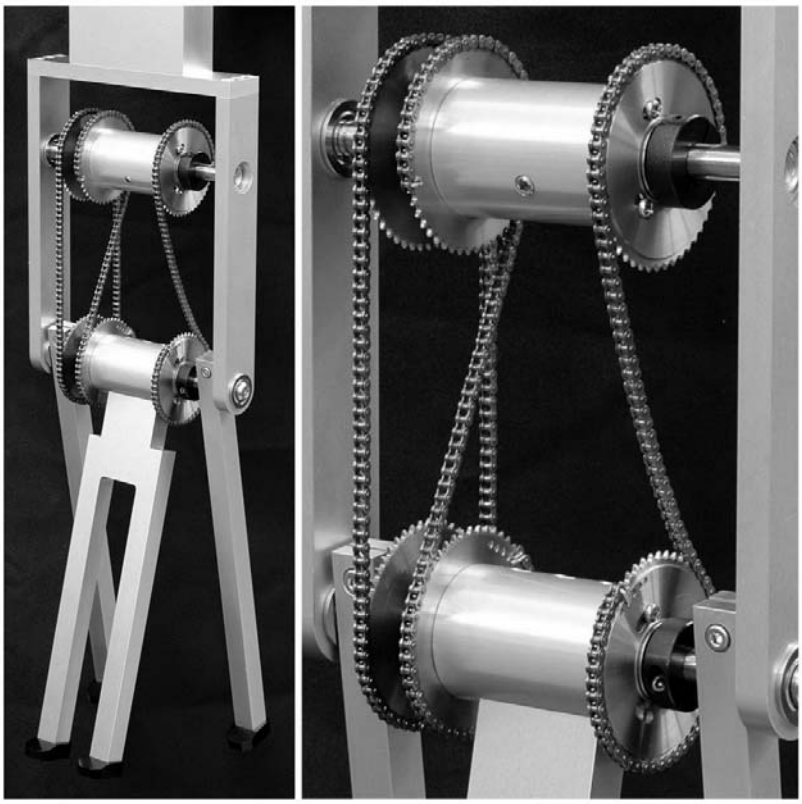

Fig. 1 Overview of prototype bisecting hip mechanism

where $\boldsymbol{J}_H^{\mathrm{T}}\lambda_H \in \mathbb{R}^3$ denotes the constraint force vector caused by the BHM. The details of $\boldsymbol{M}(\boldsymbol{\theta})$ and $\boldsymbol{h}(\boldsymbol{\theta}, \dot{\boldsymbol{\theta}})$ are as follows.

$$\boldsymbol{M}(\boldsymbol{\theta}) = \begin{bmatrix} M_{11} & M_{12} & M_{13} \\ & M_{22} & 0 \\ \text{Sym.} & & M_{33} \end{bmatrix}, \quad \boldsymbol{h}(\boldsymbol{\theta}, \dot{\boldsymbol{\theta}}) = \begin{bmatrix} h_1 \\ h_2 \\ h_3 \end{bmatrix}$$

$$\begin{aligned} M_{11} &= I + MR^2 + m_T(l-R)(l-R+2R\cos\theta_1) \\ &\quad + m\left((a-R)^2 + (l-R)^2 + 2R\,(a+l-2R)\cos\theta_1\right) \\ M_{12} &= -mb\,(R\cos\theta_2 + (l-R)\cos(\theta_1-\theta_2)) \\ M_{13} &= m_T\,(Rl_T\cos\theta_3 + l_T(l-R)\cos(\theta_1-\theta_3)) \\ M_{22} &= I + mb^2 \\ M_{33} &= I_T + m_T l_T^2 \end{aligned}$$

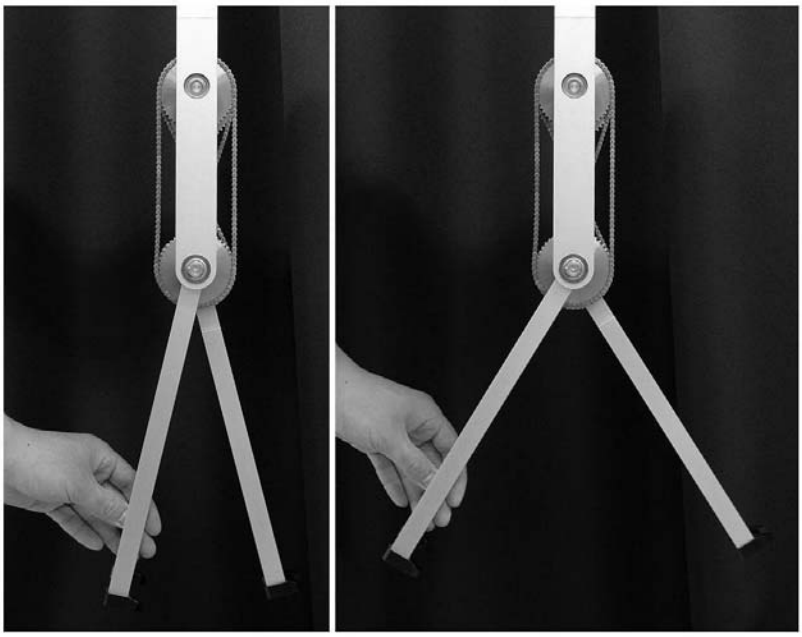

Fig. 2 Symmetric motion of legs

$$
\begin{aligned}
h_1 = & -R\dot{\theta}_1^2 \sin\theta_1 \left(m(a+l-R) + m_T(l-R)\right) \\
& + mb\dot{\theta}_2^2 \left(R\sin\theta_2 - (l-R)\sin(\theta_1-\theta_2)\right) \\
& - m_T l_T \dot{\theta}_3^2 \left(R\sin\theta_3 - (l-R)\sin(\theta_1-\theta_3)\right) \\
& - \left(m(a+l) + m_T l - MR\right) g\sin\theta_1 \\
h_2 = & \; mb(l-R)\dot{\theta}_1^2 \sin(\theta_1-\theta_2) + mbg\sin\theta_2 \\
h_3 = & -m_T l_T (l-R)\dot{\theta}_1^2 \sin(\theta_1-\theta_3) - m_T l_T g \sin\theta_3
\end{aligned}
$$

The control input vector $\boldsymbol{Su} \in \mathbb{R}^3$ is also defined as

$$
\boldsymbol{Su} = \begin{bmatrix} 1 & 0 \\ 0 & 1 \\ -1 & -1 \end{bmatrix} \begin{bmatrix} u_1 \\ u_2 \end{bmatrix}. \tag{2}
$$

The geometric relation between the torso and legs according to the BHM is given by

$$
\theta_3 = \frac{\theta_1 + \theta_2}{2}. \tag{3}
$$

The time derivative of Eq. (3) becomes

$$
\dot{\theta}_3 = \frac{\dot{\theta}_1 + \dot{\theta}_2}{2}. \tag{4}
$$

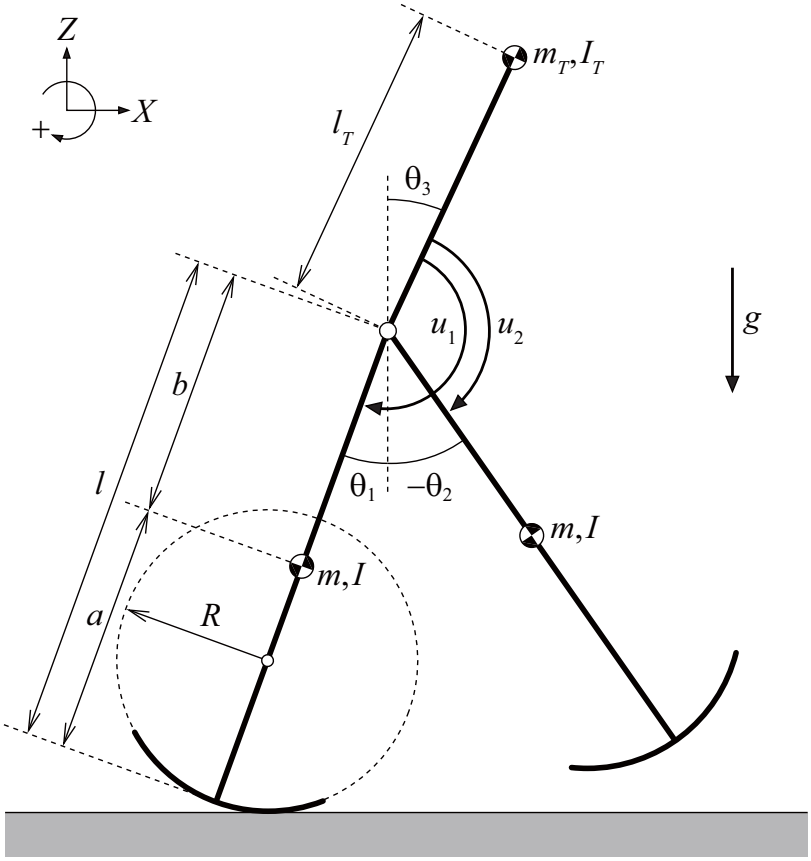

Fig. 3 Model of planar underactuated biped robot with semicircular feet and torso

This can be simply rearranged as

$$\boldsymbol{J}_H\dot{\boldsymbol{\theta}} = 0,\ \boldsymbol{J}_H = \begin{bmatrix} 1 & 1 & -2 \end{bmatrix}. \tag{5}$$

This leads to $\boldsymbol{J}_H\ddot{\boldsymbol{\theta}} = 0$, and by substituting this into Eq. (1), we obtain λ_H as

$$\lambda_H = -X_H(\boldsymbol{\theta})^{-1}\boldsymbol{J}_H\boldsymbol{M}(\boldsymbol{\theta})^{-1}\left(\boldsymbol{S}\boldsymbol{u} - \boldsymbol{h}(\boldsymbol{\theta},\dot{\boldsymbol{\theta}})\right), \tag{6}$$

$$X_H(\boldsymbol{\theta}) = \boldsymbol{J}_H\boldsymbol{M}(\boldsymbol{\theta})^{-1}\boldsymbol{J}_H^{\mathrm{T}}. \tag{7}$$

By substituting this into Eq. (1), we further simplify the robot's dynamic equation to be

$$\boldsymbol{M}(\boldsymbol{\theta})\ddot{\boldsymbol{\theta}} = \boldsymbol{Y}_H(\boldsymbol{\theta})\left(\boldsymbol{S}\boldsymbol{u} - \boldsymbol{h}(\boldsymbol{\theta},\dot{\boldsymbol{\theta}})\right), \tag{8}$$

where

$$\boldsymbol{Y}_H(\boldsymbol{\theta}) = \boldsymbol{I}_3 - X_H(\boldsymbol{\theta})^{-1}\boldsymbol{J}_H^{\mathrm{T}}\boldsymbol{J}_H\boldsymbol{M}(\boldsymbol{\theta})^{-1}. \tag{9}$$

2.3 Transition Equation

The heel-strike is modeled as an inelastic collision. We introduce the extended coordinate vector, $\boldsymbol{q}_i \in \mathbb{R}^3$, for the two legs ($i = 1$ or 2) and torso ($i = 3$): $\boldsymbol{q}_i = \left[\, x_i \; z_i \; \theta_i \,\right]^{\mathrm{T}}$. Fig. 4 shows the configuration at the instant of the heel-strike. (x_i, z_i) is the central position of Leg i's semicircular foot as shown in the figure. Let α [rad] be the half inter-leg angle at impact, that is,

$$\alpha := \frac{\theta_1^- - \theta_2^-}{2} = \frac{\theta_2^+ - \theta_1^+}{2} > 0. \tag{10}$$

Then $\theta_1^{\mp} = \theta_2^{\pm} = \alpha$ holds. In this extended coordinate, however, the stance and swing legs are not exchanged. We then express θ_i^+ and θ_i^- simply as θ_i. The augmented coordinate vector is defined as $\boldsymbol{q} = \left[\, \boldsymbol{q}_1^{\mathrm{T}} \; \boldsymbol{q}_2^{\mathrm{T}} \; \boldsymbol{q}_3^{\mathrm{T}} \,\right]^{\mathrm{T}}$, and the inelastic collision model is

$$\bar{\boldsymbol{M}}(\alpha)\dot{\boldsymbol{q}}^+ = \bar{\boldsymbol{M}}(\alpha)\dot{\boldsymbol{q}}^- - \boldsymbol{J}_I(\alpha)^{\mathrm{T}}\boldsymbol{\lambda}_I, \tag{11}$$

$$\boldsymbol{J}_I(\alpha)\dot{\boldsymbol{q}}^+ = \boldsymbol{0}_{7\times 1}, \tag{12}$$

where $\bar{\boldsymbol{M}}(\alpha) \in \mathbb{R}^{9\times 9}$ and $\boldsymbol{J}_I(\alpha) \in \mathbb{R}^{7\times 9}$ are matrix functions only of α. $\boldsymbol{\lambda}_I \in \mathbb{R}^7$ denotes the impact force on the robot. Eq. (12) implies the constraint condition of the post-impact velocities, and we describe the details in the following.

Leg 1's and Leg 2's hips are positioned the same as the Torso's, and their relations can be expressed as

$$x_1 + (l-R)\sin\theta_1 = x_3,\;\; z_1 + (l-R)\cos\theta_1 = z_3,$$
$$x_2 + (l-R)\sin\theta_2 = x_3,\;\; z_2 + (l-R)\cos\theta_2 = z_3.$$

Their time derivatives are

$$\dot{x}_1^+ + (l-R)\dot{\theta}_1^+\cos\theta_1 = \dot{x}_3^+, \tag{13}$$

$$\dot{z}_1^+ - (l-R)\dot{\theta}_1^+\sin\theta_1 = \dot{z}_3^+, \tag{14}$$

$$\dot{x}_2^+ + (l-R)\dot{\theta}_2^+\cos\theta_2 = \dot{x}_3^+, \tag{15}$$

$$\dot{z}_2^+ - (l-R)\dot{\theta}_2^+\sin\theta_2 = \dot{z}_3^+. \tag{16}$$

On the other hand, the conditions of rolling contact of Leg 2 with the ground are given by

$$\dot{x}_2^+ = R\dot{\theta}_2^+, \tag{17}$$

$$\dot{z}_2^+ = 0. \tag{18}$$

Furthermore, the constraint on the post-impact angular velocities due to the BHM is given by

$$\dot{\theta}_1^+ + \dot{\theta}_2^+ = 2\dot{\theta}_3^+. \tag{19}$$

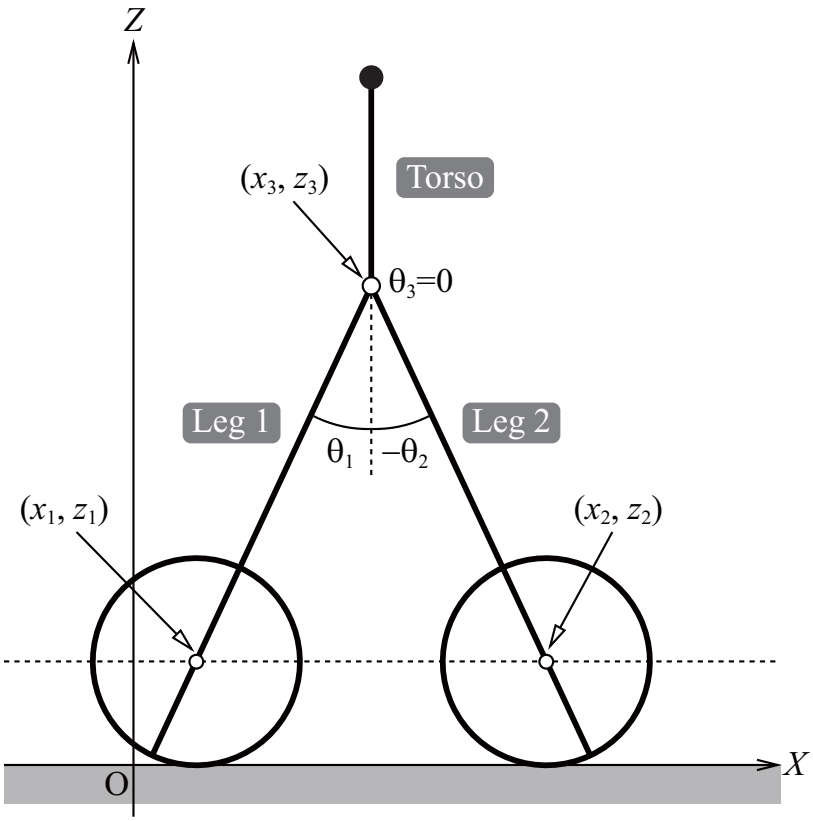

Fig. 4 Configuration at instant of heel-strike

The above seven conditions can be formulated as a matrix $\boldsymbol{J}_I(\alpha)$:

$$\boldsymbol{J}_I(\alpha) = \begin{bmatrix} 1 & 0 & J_{13} & 0 & 0 & 0 & -1 & 0 & 0 \\ 0 & 1 & J_{23} & 0 & 0 & 0 & 0 & -1 & 0 \\ 0 & 0 & 0 & 1 & 0 & J_{36} & -1 & 0 & 0 \\ 0 & 0 & 0 & 0 & 1 & J_{46} & -1 & 0 & 0 \\ 0 & 0 & 0 & 1 & 0 & -R & 0 & 0 & 0 \\ 0 & 0 & 0 & 0 & 1 & 0 & 0 & 0 & 0 \\ 0 & 0 & 1 & 0 & 0 & 1 & 0 & 0 & -2 \end{bmatrix}, \tag{20}$$

where

$$J_{13} = (l - R)\cos\theta_1, \quad J_{23} = -(l - R)\sin\theta_1,$$
$$J_{36} = (l - R)\cos\theta_2, \quad J_{46} = -(l - R)\sin\theta_2.$$

Following Eqs. (11) and (12), we get

$$\dot{\boldsymbol{q}}^{+} = \boldsymbol{Y}(\alpha)\dot{\boldsymbol{q}}^{-}, \tag{21}$$
$$\boldsymbol{Y}(\alpha) := \boldsymbol{I}_9 - \bar{\boldsymbol{M}}(\alpha)^{-1}\boldsymbol{J}_I(\alpha)^{\mathrm{T}}\boldsymbol{X}_I(\alpha)^{-1}\boldsymbol{J}_I(\alpha), \tag{22}$$
$$\boldsymbol{X}_I(\alpha) := \boldsymbol{J}_I(\alpha)\bar{\boldsymbol{M}}(\alpha)^{-1}\boldsymbol{J}_I(\alpha)^{\mathrm{T}}. \tag{23}$$

The following relationship for the velocities immediately before impact holds.

$$\dot{\boldsymbol{q}}^{-} = \boldsymbol{H}(\alpha)\dot{\boldsymbol{\theta}}^{-} = \boldsymbol{H}(\alpha)\begin{bmatrix} 1 & 0 \\ 0 & 1 \\ 1/2 & 1/2 \end{bmatrix}\begin{bmatrix} \dot{\theta}_1^{-} \\ \dot{\theta}_2^{-} \end{bmatrix} =: \boldsymbol{H}(\alpha)\boldsymbol{T}\dot{\bar{\boldsymbol{\theta}}}^{-} \tag{24}$$

Where matrix $\boldsymbol{H}(\alpha) \in \mathbb{R}^{9\times 3}$ is defined as

$$\boldsymbol{H}(\alpha) := \begin{bmatrix} R & 0 & 0 \\ 0 & 0 & 0 \\ 1 & 0 & 0 \\ R + (l-R)\cos\alpha & -(l-R)\cos\alpha & 0 \\ -(l-R)\sin\alpha & -(l-R)\sin\alpha & 0 \\ 0 & 1 & 0 \\ R + (l-R)\cos\alpha & 0 & 0 \\ -(l-R)\sin\alpha & 0 & 0 \\ 0 & 0 & 1 \end{bmatrix}.$$

Following Eqs. (21), (24), and the relation between $\dot{\boldsymbol{q}}^{+}$ and $\dot{\boldsymbol{\theta}}^{+}$, the angular velocity vector immediately after impact can then be simply expressed using $\dot{\theta}_1^{-}$ and $\dot{\theta}_2^{-}$ as follows:

$$\dot{\boldsymbol{\theta}}^{+} = \begin{bmatrix} 0&0&0&0&0&1&0&0&0 \\ 0&0&1&0&0&0&0&0&0 \\ 0&0&0&0&0&0&0&0&1 \end{bmatrix}\boldsymbol{Y}(\alpha)\boldsymbol{H}(\alpha)\boldsymbol{T}\dot{\bar{\boldsymbol{\theta}}}^{-} =: \boldsymbol{\Xi}(\alpha)\dot{\bar{\boldsymbol{\theta}}}^{-}, \tag{25}$$

where $\boldsymbol{\Xi}(\alpha) \in \mathbb{R}^{3\times 2}$ is also a function matrix of α.

2.4 Mechanical Energy

The robot's total mechanical energy is defined as the sum of kinetic and potential energies:

$$E(\boldsymbol{\theta}, \dot{\boldsymbol{\theta}}) = \frac{1}{2}\dot{\boldsymbol{\theta}}^{\mathrm{T}}\boldsymbol{M}(\boldsymbol{\theta})\dot{\boldsymbol{\theta}} + P(\boldsymbol{\theta}), \tag{26}$$

and its time derivative satisfies the following relation:

$$\dot{E} = \dot{\boldsymbol{\theta}}^{\mathrm{T}}\boldsymbol{S}\boldsymbol{u} = \left(\dot{\theta}_1 - \dot{\theta}_3\right)u_1 + \left(\dot{\theta}_2 - \dot{\theta}_3\right)u_2. \tag{27}$$

By using Eq. (4), this can be rearranged as

$$\dot{E} = \frac{\dot{\theta}_H u_1}{2} - \frac{\dot{\theta}_H u_2}{2}, \tag{28}$$

where $\theta_H := \theta_1 - \theta_2$ is the relative hip-joint angle. Eq. (28) implies that the two control torques, u_1 and u_2, drive the same joint inversely. The walking system shown in Fig. 3 virtually has 2-DOF and one control torque due to the mechanical constraint of the BHM. The complexity of the driving mechanism is simplified; this idea can be found in the study of Grishin et al. [8] In the subsequent sections, we assume $u_2 = 0$ for simplicity.

2.5 Energy Efficiency

The energy efficiency of a walking robot can be evaluated in terms of specific resistance $:= p/Mgv$ [-], which implies an expenditure of energy per unit mass and per unit length traveled. $M := m_T + 2m$ [kg] is the robot's total mass, and $g = 9.81$ [m/s^2] is the gravity acceleration. p [J/s] is the average input power defined as

$$p := \frac{1}{T}\int_{0^+}^{T^-} \frac{\left|\dot{\theta}_H u_1\right| + \left|\dot{\theta}_H u_2\right|}{2} \mathrm{d}t, \tag{29}$$

and v [m/s] is the average walking speed defined as

$$v := \frac{1}{T}\int_{0^+}^{T^-} \dot{X}_g \ \mathrm{d}t = \frac{\Delta X_g}{T}, \tag{30}$$

where T [s] is the steady step period, X_g [m] is the X-position of the center of mass (CoM), and $\Delta X_g := X_g(T^-) - X_g(0^+)$ [m] is the horizontal displacement of the CoM and is equal to the step. In the following, we simply call X_g CoM.

3 Pseudo Virtual Passive Dynamic Walking and Its Extensions

3.1 Formulation Using Pseudo CoM

In VPDW, the time rate of change of mechanical energy during stance phases satisfies the following relation:

$$\dot{E} = \frac{\dot{\theta}_H u_1}{2} = Mg\tan\phi\dot{X}_g, \tag{31}$$

where $M := m_H + 2m$ [kg] is the robot total mass and ϕ [rad] is the virtual slope angle [1]. The control input is then specified from Eq. (31) as

$$u_1 = \frac{2Mg\tan\phi\dot{X}_g}{\dot{\theta}_H}. \tag{32}$$

On the other hand, by integrating Eq. (31) with respect to time, we obtain the following relation:

$$\Delta E = Mg\tan\phi\Delta X_g, \tag{33}$$

where ΔE [J] is the restored mechanical energy and ΔX_g [m], which is equivalent to the step length, satisfies the following relation:

$$\Delta X_g := X_g(T^-) - X_g(0^+) = 2\left(R\alpha + (l-R)\sin\alpha\right). \tag{34}$$

$t = 0^+$ and T^- [s] stand for the time instants immediately after impact and immediately before the next impact. The control input of Eq. (32) has a singularity of $\dot{\theta}_H = 0$, and the biped system then behaves unnaturally around the singular point. The maximum control input also becomes large with it. We then reconsider this approach and introduce the following control input, u_1:

$$u_1 = Mg\tan\phi\left(R + (l-R)\cos\frac{\theta_H}{2}\right). \tag{35}$$

By substituting this and $u_2 = 0$ into Eq. (31) and integrating it with respect to time, we get

$$\begin{aligned}\frac{\Delta E}{Mg\tan\phi} &= \int_{0^+}^{T^-} \frac{\dot{\theta}_H}{2}\left(R + (l-R)\cos\frac{\theta_H}{2}\right)\mathrm{d}t \\ &= \left[\frac{R\theta_H}{2} + (l-R)\sin\frac{\theta_H}{2}\right]_{\theta_H=-2\alpha}^{\theta_H=2\alpha} \\ &= 2\left(R\alpha + (l-R)\sin\alpha\right) = \Delta X_g. \end{aligned} \tag{36}$$

This satisfies the relation of Eq. (33). In this sense, the authors called the walking style driven by this control input *pseudo virtual passive dynamic walking* (PVPDW).

In this paper, we further consider the mathematical formulation during stance phases. Define the pseudo CoM as

$$\hat{X_g} := \frac{R\theta_H}{2} + (l-R)\sin\frac{\theta_H}{2}, \tag{37}$$

and its time-derivative satisfies

$$\dot{\hat{X}}_g = \frac{\dot{\theta}_H}{2}\left(R + (l-R)\cos\frac{\theta_H}{2}\right) = \frac{\dot{\theta}_H}{2}\cdot\frac{u_1}{Mg\tan\phi} = \frac{\dot{E}}{Mg\tan\phi}. \tag{38}$$

This leads to

$$\frac{\partial E}{\partial \hat{X}_g} = Mg\tan\phi, \tag{39}$$

and we can find that Eq. (39) is in the same formula of VPDW. In addition, following Eq. (33), the minimum value of specific resistance (SR) becomes $\mathrm{SR} \geq \tan\phi$ which is the same as that of VPDW [1].

3.2 Linearization and Energy-efficiency

By linearizing the pseudo CoM given by Eqs. (37) and (38) and the control input of Eq. (35) around $\theta_H = 0$, we obtain

$$\hat{X}_g = \frac{l\theta_H}{2}, \quad \dot{\hat{X}}_g = \frac{l\dot{\theta}_H}{2}, \quad u_1 = Mlg\tan\phi. \tag{40}$$

Also in this case, the relation of Eq. (39) holds. The physical meaning of PVPDW is more simplified; the robot is driven by a constant torque of Eq. (40), and the mechanical energy is then restored proportional to the change of hip angle.

The restored mechanical energy in this case becomes

$$\Delta E = \int_{0^+}^{T^-} \frac{\dot{\theta}_H u_1}{2}\mathrm{d}t = \frac{Mlg\tan\phi}{2}\int_{-2\alpha}^{2\alpha}\mathrm{d}\theta_H = 2l\alpha Mg\tan\phi = Mg\tan\phi\Delta\hat{X}_g, \tag{41}$$

and following Eqs. (36) and (41), SR satisfies the following magnitude relation:

$$\mathrm{SR} \geq \frac{\Delta E}{Mg\Delta X_g} = \frac{l\alpha\tan\phi}{R\alpha + (l-R)\sin\alpha}. \tag{42}$$

Further, considering that the denominator of Eq. (42) satisfies

$$R\alpha + (l-R)\sin\alpha < R\alpha + (l-R)\alpha = l\alpha \tag{43}$$

if $0 < \alpha < \pi/2$, we can conclude $\mathrm{SR} > \tan\phi$. Although the equality does not hold as in the case of VPDW, the difference is quite small as described later.

4 Swing-leg Retraction and Its Control

4.1 Quasi-constraint on Impact Posture

Limit cycle walkers often exhibit *swing-leg retraction* (SLR), which is the motion of the swing leg; it moves backward immediately prior to heel strike [3]. It is mathematically explained as follows. The sign of angular velocity of the relative hip joint, $\dot{\theta}_H$, changes from positive to negative immediately prior to impact. This phenomenon is often observed in passive or semi-passive dynamic gaits. The author found that inhibiting SLR improves biped gait stability through numerical analysis. We describe the details in the following.

We consider to constraint the hip joint mechanically at the instant of $\dot{\theta}_H = 0$. This constraint condition is mathematically expressed as $\dot{\theta}_1 = \dot{\theta}_2$, that is,

$$\boldsymbol{J}_Q\dot{\boldsymbol{\theta}} = \begin{bmatrix} 1 & -1 & 0 \end{bmatrix}\dot{\boldsymbol{\theta}} = 0.$$

This effect is added to the walking system together with the BHM constraint as

$$\boldsymbol{M}(\boldsymbol{\theta})\ddot{\boldsymbol{\theta}} + \boldsymbol{h}(\boldsymbol{\theta},\dot{\boldsymbol{\theta}}) = \boldsymbol{J}_H^{\mathrm{T}}\lambda_H + \boldsymbol{J}_Q^{\mathrm{T}}\lambda_Q, \tag{44}$$

where $\lambda_Q \in \mathbb{R}$ is an undetermined multiplier for the holonomic constraint force. The control input, u_H, then becomes zero during this phase.

We call this active hip-locking *quasi-constraint on impact posture* in the sense that the target hip angle is not precisely given. In general, we must control the hip angle to follow the desired-time trajectory to achieve the constraint on impact posture [9][10], whereas the quasi-constraint achieves only keeping the angular velocity of hip-joint zero. By this constraint, we can avoid inefficiency due to the negative input-power because $\dot{\theta}_H u_1 \geq 0$ is always achieved.

4.2 Typical Steady Gait

Fig. 5 shows a typical steady gait of PVPDW with quasi-constraint on impact posture where $\phi = 0.01$ [rad]. Fig. 6 shows the snapshots of the steady walking motion. Table 1 lists the physical parameters. In the simulation program, we switched the robot dynamic equation from Eq. (1) to (44) at the instant of $\dot{\theta}_H = 0$. From Fig. 5 (b), we can confirm that quasi-constraint is achieved because all the angular velocities are kept in the same orbit. Fig. 5 (c) shows the time evolutions of the CoM and pseudo CoM, and they greatly differ from each other. As expected from Eq. (40), the pseudo CoM behaves in the same way as the relative hip angle does; it monotonically increases during swing phases.

Table 1 Physical parameters of biped robot

m_T	10.0	kg
m	5.0	kg
I_T	0.001	kg·m^2
I	0.001	kg·m^2

l_T	0.3	m
$l\ (= a + b)$	1.0	m
a	0.5	m
b	0.5	m
R	0.3	m

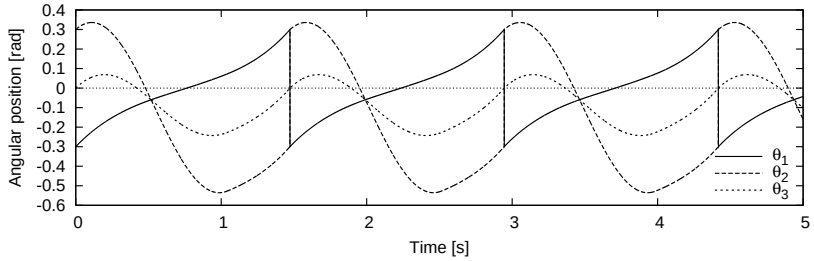

(a) Angular position

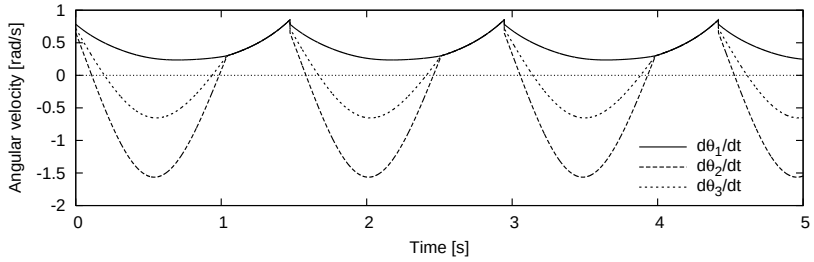

(b) Angular velocity

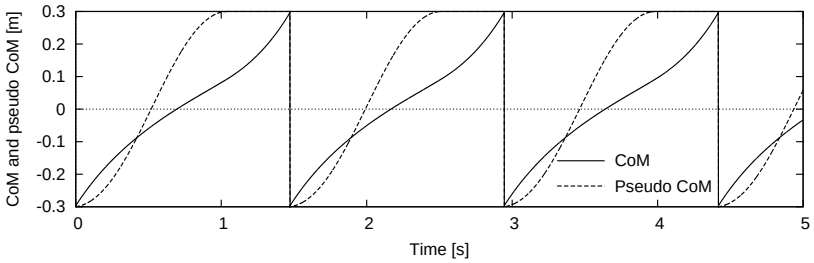

(c) CoM and pseudo CoM

Fig. 5 Simulation results for pseudo virtual passive dynamic walking with quasi constraint on impact posture where $\phi = 0.01$ [rad]

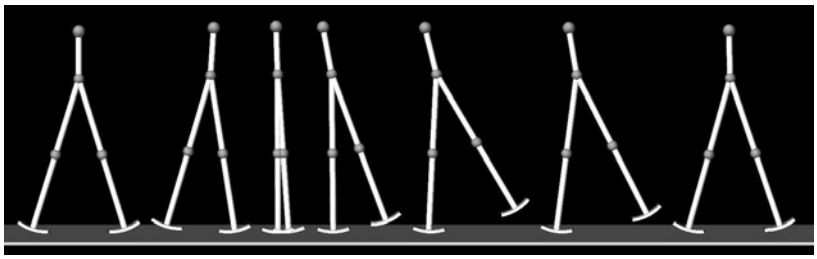

Fig. 6 One cycle of motion for pseudo virtual passive dynamic walking with quasi-constraint on impact posture

4.3 Robust Energy Control

The authors proposed a robust control method termed as *the robust energy control* based on the property of mechanical energy restoration in VPDW [1]. Let us apply this control to the PVPDW system. We consider the following formula:

$$\dot{E} = \frac{\dot{\theta}_H u_1}{2} = Mg\tan\phi\dot{\hat{X}}_g - \zeta\left(E - E_{\rm d}(\hat{X}_g)\right)\dot{\hat{X}}_g. \tag{45}$$

This is formulated to satisfy the relation

$$\frac{\partial E}{\partial \hat{X}_g} = Mg\tan\phi - \zeta\left(E - E_{\rm d}(\hat{X}_g)\right), \tag{46}$$

which is found to be a trajectory tracking system not with respect to time but with respect to the pseudo CoM. From Eq. (45) and the second equation in Eq. (40), u_1 yields the following form without having any singularities.

$$u_1 = Mlg\tan\phi - \zeta l\left(E - E_{\rm d}(\hat{X}_g)\right) \tag{47}$$

This control input is time-independent and does not have singularities. Here, $\zeta > 0$ is the feedback gain and $E_{\rm d}$ is the desired trajectory of mechanical energy which is given as a linear function of the pseudo CoM, $\hat{X}_g$, as follows:

$$E_{\rm d}(\hat{X}_g) = E_0 + Mg\tan\phi\hat{X}_g. \tag{48}$$

Where E_0 [J] is the desired value of mechanical energy when $\hat{X}_g = 0$ and is uniquely determined in accordance with the steady generated gait. We must conduct numerical simulation to obtain this value precisely, or the control input does not converge to the constant value of Eq. (40). The effect of robust stabilization is, however, expectable even if there is a small margin of error.

Fig. 7 shows the simulation results for robust energy control with the same parameter settings. Fig. 7 (a) shows the mechanical energy with respect to the pseudo CoM. The robot started from an initial condition close to the steady value. In this case, $E_0 = 179.17$ [J] and $\zeta = 10.0$. Although we omit the details on the simulation results, we confirmed that the convergence speed to the steady gait increases and the stability of limit cycle improved. Fig. 7 (b) shows the time evolution of u_1. At the start of walking, the amount of the energy feedback control is added to the constant torque of $Mlg\tan\phi$. It then converges to the constant torque as the gait converges to the steady one.

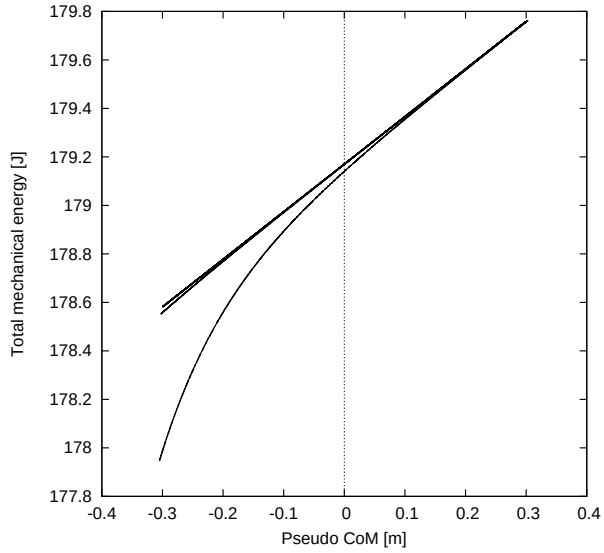

(a) Total mechanical energy versus pseudo CoM

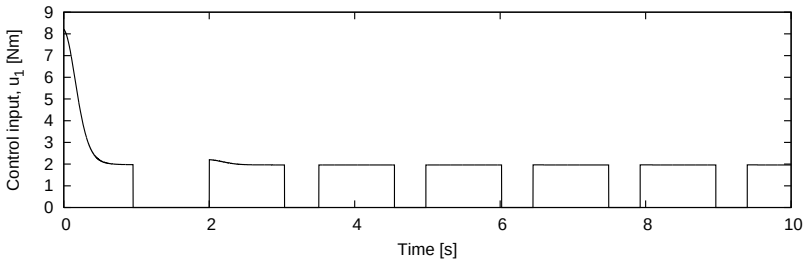

(b) Time evolution of u_1

Fig. 7 Simulation results of robust energy control

5 Gait Analysis

5.1 Gait Properties

This subsection analyzes the gait efficiency and stable domain. Fig. 8 shows the change of gait descriptors with respect to l_T in the cases with quasi-constraint and without it where $\phi = 0.01$ [rad]. Here, (a) is the walking speed, (b) the specific resistance, and (c) the step length. The physical parameters except l_T were chosen as listed in Table 1. From Fig. 8 (a), we can confirm that the walking speeds monotonically decrease with the increase of l_T due to the effect of upper body as a counterweight. It is also observed that period-doubling bifurcation occurs in the case without quasi-constraint. From Fig. 8 (b), we can see that the SR in the generated gait without quasi-constraint is significantly worse than that with it. This is caused by negative input power

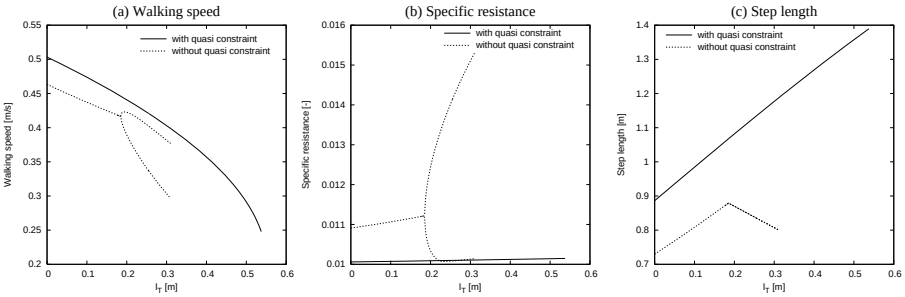

Fig. 8 Gait descriptors with respect to l_T

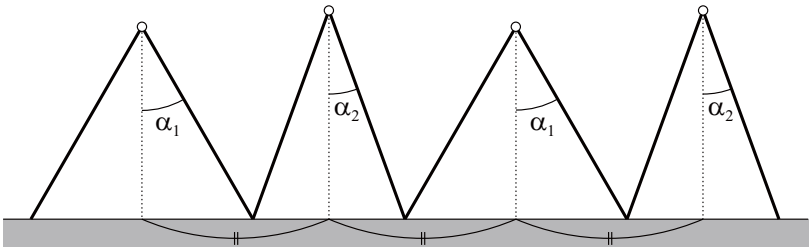

Fig. 9 Steady 2-period gait and its constant step length

during SLR. From Fig. 8 (c), we can see that the step length does not bifurcate even if the gait becomes 2-period. Fig. 9 strongly supports the geometrical reason. It should be remarked that the step length changes to decrease after exceeding the first bifurcation point. In other words, the pace slows after the point on average. By controlling SLR, however, we can avoid the bifurcation and slowing down of pace.

5.2 Convergence of Limit Cycle

In this paper, we analyze the limit cycle stability from the viewpoint of energy-loss coefficient, which is defined as

$$\varepsilon = \frac{K^+}{K^-}, \tag{49}$$

where K^+ and K^- [J] are kinetic energies immediately after and immediately before impact. They are respectively given by

$$K^+ = \frac{1}{2}\left(\dot{\boldsymbol{\theta}}^+\right)^{\mathrm{T}} \boldsymbol{M}(\alpha)\dot{\boldsymbol{\theta}}^+, \quad K^- = \frac{1}{2}\left(\dot{\boldsymbol{\theta}}^-\right)^{\mathrm{T}} \boldsymbol{M}(\alpha)\dot{\boldsymbol{\theta}}^-. \tag{50}$$

According to the quasi-constraint on impact posture, the energy-loss coefficient depends only on the half inter-leg angle, α, and does not depend on the angular velocities as described later. In addition, $0 < \varepsilon < 1$ holds due to the magnitude relation of $0 < K^+ < K^-$.

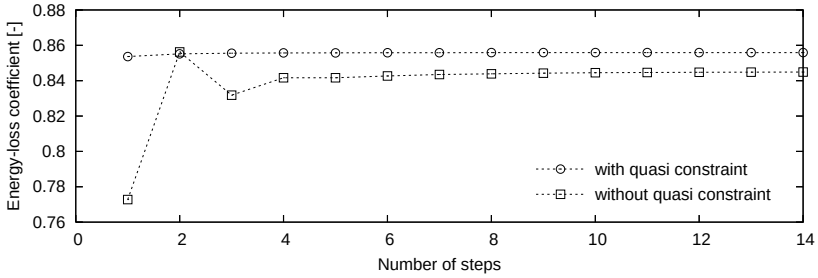

Fig. 10 Convergence of energy-loss coefficients

Fig. 10 plots the convergence of energy-loss coefficients in the cases with quasi-constraint and without it. In both cases, the robot started from the same initial condition but their steady gaits converged to different limit cycles. We can see that the convergence speed in the case with quasi-constraint is significantly rapider than that without quasi-constraint. This implies that falling as a 1-DOF rigid body dramatically improves the gait stability in the sense of increasing the convergence speed even if the target hip angle at impact is not precisely given.

We must achieve both constraint on impact posture and on restored mechanical energy simultaneously to guarantee the asymptotic stability as a rimless wheel [9]. Only by falling as a 1-DOF rigid body, however, the stable domain and convergence speed are dramatically improved simultaneously.

5.3 Energy-loss Coefficient

Considering the relations of Eqs. (24) and (25), the kinetic energies immediately after and immediately before impact in Eq. (50) can be arranged as

$$K^+ = \frac{1}{2}\left(\dot{\boldsymbol{\theta}}^-\right)^{\mathrm{T}} \boldsymbol{\Xi}(\alpha)^{\mathrm{T}} \boldsymbol{M}(\alpha) \boldsymbol{\Xi}(\alpha) \dot{\boldsymbol{\theta}}^-, \tag{51}$$

$$K^- = \frac{1}{2}\left(\dot{\boldsymbol{\theta}}^-\right)^{\mathrm{T}} \boldsymbol{T}^{\mathrm{T}} \boldsymbol{M}(\alpha) \boldsymbol{T} \dot{\boldsymbol{\theta}}^-. \tag{52}$$

Let $\|\cdot\|$ be a vector norm and define $\hat{\boldsymbol{M}}(\alpha)^{\pm} \in \mathbb{R}^{2\times 2}$ as follows.

$$\hat{\boldsymbol{M}}^{+}(\alpha) := \boldsymbol{\Xi}(\alpha)^{\mathrm{T}} \boldsymbol{M}(\alpha) \boldsymbol{\Xi}(\alpha), \quad \hat{\boldsymbol{M}}^{-}(\alpha) := \boldsymbol{T}^{\mathrm{T}} \boldsymbol{M}(\alpha) \boldsymbol{T}$$

$K^{\pm}$ is then arranged as

$$K^{\pm} = \frac{1}{2}\left\| \boldsymbol{M}^{\pm}(\alpha)^{\frac{1}{2}} \dot{\boldsymbol{\theta}}^- \right\|^2. \tag{53}$$

Here, let us define

$$\boldsymbol{x} := \hat{\boldsymbol{M}}^{-}(\alpha)^{\frac{1}{2}} \dot{\boldsymbol{\theta}}^-. \tag{54}$$

K^+ is then able to be rearranged as

$$K^+ = \frac{1}{2}\left\|\hat{\boldsymbol{M}}^+(\alpha)^{\frac{1}{2}}\hat{\boldsymbol{M}}^-(\alpha)^{-\frac{1}{2}}\boldsymbol{x}\right\|^2, \tag{55}$$

and energy-loss coefficient becomes

$$\varepsilon = \frac{K^+}{K^-} = \frac{\|\boldsymbol{\Omega}\boldsymbol{x}\|^2}{\|\boldsymbol{x}\|^2}, \tag{56}$$

where matrix $\boldsymbol{\Omega} \in \mathbb{R}^{2\times 2}$ is defined as

$$\boldsymbol{\Omega} := \hat{\boldsymbol{M}}^+(\alpha)^{\frac{1}{2}}\hat{\boldsymbol{M}}^-(\alpha)^{-\frac{1}{2}}. \tag{57}$$

As the generated gait converges to a 1-period limit cycle, ε also converges to a constant. The range of the value can be calculated by calculating the singular value of matrix $\boldsymbol{\Omega}$ as mentioned later.

In the case with quasi-constraint on impact posture, the relation

$$\dot{\boldsymbol{\theta}}^- = \boldsymbol{T}\begin{bmatrix}1\\1\end{bmatrix}\dot{\theta}_1^- \tag{58}$$

holds because of $\dot{\theta}_1^- = \dot{\theta}_2^-$. By substituting this into Eq. (50), we get

$$K^+ = \frac{1}{2}\bar{M}^+\left(\dot{\theta}_1^-\right)^2,\ K^- = \frac{1}{2}\bar{M}^-\left(\dot{\theta}_1^-\right)^2, \tag{59}$$

where $\bar{M}^+ \in \mathbb{R}$ and $\bar{M}^- \in \mathbb{R}$ are positive scalar functions of α, and are respectively defined as

$$\bar{M}^+ := \begin{bmatrix}1\\1\end{bmatrix}^{\mathrm{T}}\boldsymbol{\Xi}^{\mathrm{T}}\boldsymbol{M}(\alpha)\boldsymbol{\Xi}\begin{bmatrix}1\\1\end{bmatrix}, \tag{60}$$

$$\bar{M}^- := \begin{bmatrix}1\\1\end{bmatrix}^{\mathrm{T}}\boldsymbol{M}(\alpha)\begin{bmatrix}1\\1\end{bmatrix}. \tag{61}$$

Eq. (59) then leads to

$$\varepsilon = \frac{\bar{M}^+}{\bar{M}^-} =: \varepsilon_0,$$

and this shows that ε_0 does not depend on the angular velocities immediately before impact. It depends only on α, i.e. $\varepsilon_0 = \varepsilon_0(\alpha)$. Whereas in the case without quasi-constraint on impact posture, $\varepsilon = \varepsilon(\alpha, \dot{\boldsymbol{\theta}}^-)$ and its range of value is

$$0 < \sigma_2(\boldsymbol{\Omega})^2 \le \varepsilon \le \sigma_1(\boldsymbol{\Omega})^2 < 1, \tag{62}$$

where σ_1 and σ_2 are the maximum and minimum singular values of $\boldsymbol{\Omega}$. $\varepsilon = 0$ gives the highest convergence speed in the sense of deadbeat control, but the generated gait is inefficient because this implies that the energy-loss at impact is maximum. In contrast, $\varepsilon = 1$ implies that the convergence speed is worst but the energy-loss is minimum.

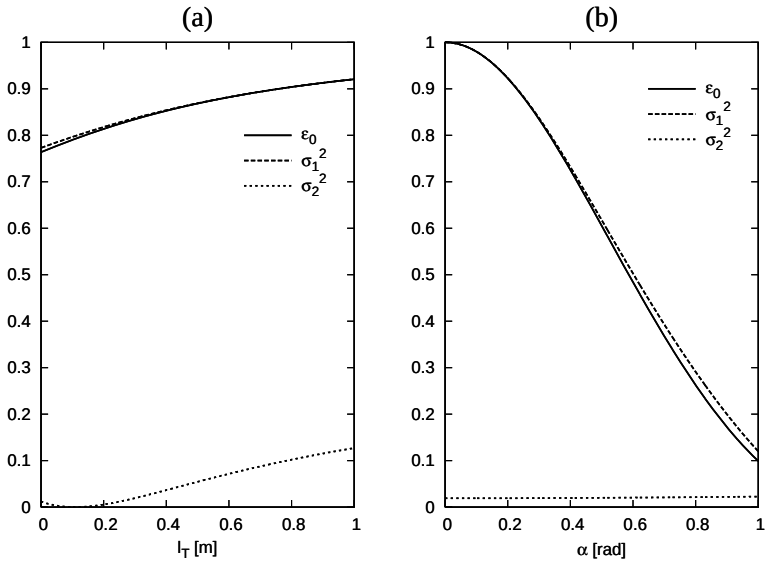

Fig. 11 Plots of σ_1, σ_2 and ε_0 with respect to l_T and α

Fig. 11 plots σ_1^2, σ_2^2 and ε_0. Here, (a) is those with respect to l_T and (b) those with respect to α. The physical parameters except l_T in (a) were chosen as listed in Table 1.

From the results, we can see that the inequality of Eq. (62) holds and $\varepsilon_0 \approx \sigma_1(\boldsymbol{\Omega})$. In other words, quasi-constraint almost maximizes the shock-absorbing effect at impact. Whereas σ_2^2 is considerably smaller than ε_0 and σ_1^2. This is outlined as follows. Let $\nu := \dot{\theta}_2^- / \dot{\theta}_1^-$ [-] be the ratio of angular velocities immediately before impact. Then ε can be formed as a function only of ν if the physical parameters are fixed. After $\nu = 1$, i.e. quasi-constraint, ε begins to decrease rapidly with the increase of ν. ε can take σ_2^2 in the case that $\dot{\theta}_2^-$ is substantially greater than $\dot{\theta}_1^-$, that is, SLR strongly occurs. See our previous paper [11] for further details.

As described in [12], the shock-absorbing effect increases as the vertical position of CoM increases, which is supported by Fig. 11 (a). It was also described in [12] that the shock-absorbing effect increases as α decreases. This is supported by Fig. 11 (b). Since the rate of change with respect to α is large, we should control the magnitude of hip angle as constant as possible although it is not accurate.

6 Conclusion and Future Work

In this paper, we have specified PVPDW inhibiting SLR that can generate the control input without concern for the singularity and have confirmed its effectiveness through numerical simulations. The simulation results showed that

the stable domain and convergence speed are improved simultaneously. We mathematically discussed the mechanism from the energy-loss coefficient point of view. The singular value analysis showed that the energy-loss coefficient is almost maximized by applying quasi-constraint. It was also remarkable that the bifurcation (gait asymmetrization) in the case without quasi-constraint decreases the gait efficiency.

In the future, we should try to theoretically clarify the relation between bifurcation and efficiency deterioration. In the presence of SLR, however, we must note that it is impossible to formulate a 2-period gait using an asymmetric rimless wheel model [10]. Although complicated analysis is unavoidable, investigations of SLR would help to deeply understand the stability principle inherent in limit cycle walking.

Acknowledgements The authors wish to thank ONO-DENKI CO., LTD. for many helpful suggestions and technical supports in development of the prototype bisecting hip mechanism.

References

1. F. Asano, Z.-W. Luo and M. Yamakita, "Biped gait generation and control based on a unified property of passive dynamic walking," *IEEE Trans. on Robotics*, Vol. 21, No. 4, pp. 754–762, 2005.
2. F. Asano and Z.-W. Luo, "Efficient dynamic bipedal walking using effects of semicircular feet," *Robotica*, Vol. 29, Issue 3, pp. 351–365, May 2011.
3. A. Seyfarth, H. Geyer and H. Herr, "Swing-leg retraction: a simple control model for stable running," *J. of Experimental Biology*, Vol. 206, pp. 2547–2555, 2003.
4. M. Wisse, C. G. Atkeson, and D. K. Kloimwieder, "Swing leg retraction helps biped walking stability," *Proc. of the IEEE-RAS Int. Conf. on Humanoid Robots*, pp.295–300, 2005.
5. D. G. E. Hobbelen and M. Wisse, "Swing-leg retraction for limit cycle walkers improves disturbance rejection," *IEEE Trans. on Robotics*, Vol. 24, No. 2, pp. 377–389, 2008.
6. Y. Ikemata, A. Sano and H. Fujimoto, "A physical principle of gait generation and its stabilization derived from mechanism of fixed point," *Proc. of the IEEE Int. Conf. on Robotics and Automation*, pp. 836–841, May 2006.
7. Y. Kato, Y. Ikemata, A. Sano, Y. Hayashi and H. Fujimoto, "A basic study for passive walking that added upper body by means of spring mechanism," *Proc. of the 13th Int. Conf. on Climbing and Walking Robots and the Support Technologies for Mobile Machines*, pp. 753–760, Sept. 2010.
8. A. A. Grishin, A. M. Formal'ski, A. V. Lensky and S. V. Zhitomirsky, "Dynamic walking of a vehicle with two telescopic legs controlled by two drives," *Int. J. of Robotics Research*, Vol. 13, No. 2, pp. 137–147, April 1994.
9. F. Asano and Z.-W. Luo, "Asymptotically stable biped gait generation based on stability principle of rimless wheel," *Robotica*, Vol. 27, Issue 6, pp. 949–958, Oct. 2009.
10. F. Asano, "Efficiency and optimality of two-period limit cycle walking," *Advanced Robotics*, Vol. 26, No. 1-2, pp. 155–176, Jan. 2012.
11. F. Asano, "Effects of swing-leg retraction and mass distribution on energy-loss coefficient in limit cycle walking," *Proc. of the IEEE/RSJ Int. Conf. on Intelligent Robots and Systems*, pp. 3214–3219, 2009.
12. F. Asano and Z.-W. Luo, "Asymptotic stability of dynamic bipedal gait with constraint on impact posture," *Proc. of the IEEE Int. Conf. on Robotics and Automation*, pp. 1246–1251, 2008.